Catalysis Today 141 (2009) 3–11

Contents lists available at ScienceDirect

Catalysis Today

journal homepage: www.elsevier.com/locate/cattod

Selective oxidations over zeolite- and mesoporous silica-based catalysts: Selected examples☆

Paul Ratnasamy *, Darbha Srinivas

National Chemical Laboratory, Pune 411008, India

ARTICLE INFO

Article history:
Available online 23 May 2008

Keywords:
Selective oxidation
Zeolite-encapsulated metal complexes
Mn-Salen
Titanosilicates
Oxidation of hydrocarbons and limonene
Reactive oxo species

ABSTRACT

Selective oxidation of hydrocarbons/terpenes in the liquid phase are reported over three categories of zeolite- and mesoporous silica-based catalysts: (1) transition metal complexes (metal phthalocyanines, copper acetate dimers and Co/Mn acetate trimer) encapsulated in zeolite-Y, (2) transition metal complexes (Mn-Salen), grafted on SBA-15, and (3) transition metal ions in framework positions of zeolites and mesoporous molecular sieves like Ti-silicates. Upon heterogenization, the metal complexes exhibited enhanced catalytic acitivity/selectivity. The causes for the enhanced catalytic activity/product selectivity have been explored. Dimer formation (copper acetate) or geometric distortion in the zeolite cavities (metal phthalocyanines) and consequent changes in energy levels and redox potentials are shown to modify the catalytic activity (in the selective oxidation of hydrocarbons) of the encapsulated metal complexes. In the case of Mn-Salen grafted on SBA-15, increasing the acidity of the siliceous surface (by $-SO_3H$ groups, for example) leads to a more facile reduction of the Mn ions and, thereby, enhanced catalytic activity in the selective epoxidation of limonene. When Ti ions are introduced in framework positions, reactive metal-oxo species are formed on contact with H_2O_2 or O_2, which influence the mode of O–O cleavage (heterolytic/homolytic) and product selectivity. The structure–function relationships in these catalysts are reported.

1. Introduction

Selective oxidation of hydrocarbons at mild conditions with eco-friendly oxidants like molecular oxygen and H_2O_2 is still a challenging area in catalysis research. In the pursuit of mimicking metalloenzymes for their efficient catalytic activity/selectivity, catalysis researchers have immobilized several homogeneous metal complexes including those of amines, bipyridine, Schiff bases, porphyrins and phthalocyanines inside the pores of zeolites and molecular sieves either by encapsulation or grafting techniques [1–8]. In these hybrid materials, the metal complexes mimic, functionally, the active sites in the metalloenzymes. The surrounding zeolite and silica matrix provides, like the protein moiety in metalloenzymes, the necessary hydrophobic environment for the selective oxidations to occur. The heterogenized metal complexes possess the dual advantages of both the homogeneous (definite molecular structure, site isolation, etc.) and heterogeneous (easy catalyst separation and isolation, ruggedness, reusability, etc.) catalysts. Often, they exhibit enhanced catalytic activities/selectivities compared to the corresponding "neat" complexes [1–8]. In metalloenzymes, the active metal center possesses an unusual molecular geometry, electronic structure and redox properties as imposed by the protein environment [9]. Does such an unusual electronic structure of the active metal center occur even in the zeolite-mimics of enzymes and, if so, is it one of the causes of the enhanced catalytic activity of the heterogenized complexes compared to the corresponding "neat" metal complexes? Here, we present an account of our recent investigations in this area. Three categories of zeolite- and mesoporous silica-based molecular sieve catalysts, viz. (1) transition metal complexes (metal phthalocyanines, copper acetate dimer and Co/Mn acetate trimer) encapsulated in zeolite-Y, (2) Mn-Salen grafted on mesoporous SBA-15 molecular sieves, and (3) transition metal ions in framework positions of zeolites and mesoporous molecular sieves like Ti-silicates are studied. Oxidation of hydrocarbons was conducted at ambient conditions. The structures of the heterogenized metal complexes were determined using spectroscopic techniques including electron paramagnetic resonance (EPR) and diffuse reflectance UV–visible (DRUV–vis). Structure–function relationships in these catalyst systems are reported.

☆ This forms part of the plenary lecture delivered in the symposium.

* Corresponding author. Tel.: +91 20 25902018; fax: +91 20 25902633.
E-mail address: p.ratnasamy@ncl.res.in (P. Ratnasamy).

0920-5861/$ – see front matter © 2008 Elsevier B.V. All rights reserved.
doi:10.1016/j.cattod.2008.03.009

2. Experimental

2.1. Materials

The zeolite-encapsulated metal phthalocyanine complexes were prepared by the "zeolite" [10,11] and "in situ ligand" [12] synthesis methods. The zeolite encapsulated copper acetate dimer [13,14] and Co/Mn cluster complexes [15,16] were prepared by the "flexible ligand synthesis" method. In the preparation of SBA-15 grafted Mn(Salen) [17,18], the surface silanol (Si-OH) groups of SBA-15 were first condensed with 3-aminopropyltrimethoxysilane (APTMS) or 3-mercaptopropyltrimethoxysilane (MPTMS) yielding SBA-15-*pr*-NH_2 or SBA-15-*pr*-SH, respectively. Oxidation of the thiol groups in SBA-15-*pr*-SH gave rise to propylsulfonic acid-functionalized SBA-15 (SBA-15-*pr*-SO_3H). Mn(Salen)Cl was then immobilized on these functionalized surfaces and three types grafted Mn(Salen) complexes viz., SBA-15-*pr*-NH_2-Mn(Salen)Cl, SBA-15-*pr*-SH-Mn(Salen)Cl and SBA-15-pr-SO_3H-Mn(Salen)Cl were synthesized as described earlier [18]. Titanosilicates (TS-1, Ti-β, Ti-MCM-41, Ti-SBA-15, ETS-10 and amorphous Ti-SiO_2) were prepared by the hydrothermal synthesis method [19,20].

2.2. Characterization

The materials were characterized by various physicochemical techniques as described earlier [12–20]. EPR spectra of the solid catalysts were recorded on a Bruker EMX spectrometer operating at X-band frequency and a 100 kHz field modulation. Ti-oxo species were generated by contacting titanosilicates with H_2O_2 or (H_2 + O_2) [21]. In these experiments, a known quantity of titanosilicate (40 mg) was taken in quartz EPR tubes. H_2O_2 (50%, 0.1 ml) was added to it in amounts adequate to wet the solid completely. Electrochemical studies on SBA-15 grafted Mn(salen) were performed using a three-electrode system (Solatron SI-1287 electrochemical interface) [18]. The immobilized Mn complex (60 wt%) and graphite powder were mixed with 0.1 ml of Teflon powder. The slurry was then pasted on a Pt disc (1.5 mm diameter) and dried under an infrared (IR) lamp. This modified Pt disc was used as the working electrode. Pure Pt foil was used as a counter electrode and a Pt wire was used as the reference electrode. All these three electrodes were placed in a glass compartment containing DMF. $LiClO_4$ (0.1 M) was used as a supporting electrolyte.

2.3. Reaction procedures

2.3.1. Aerial oxidation of methane and cyclohexane

The reactions over zeolite-encapsulated metal phthalocyanine complexes were conducted using molecular oxygen (air) as an oxidant and *tert*-butyl hydroperoxide (70% aq. TBHP solution; equivalent to 1–3% by weight of the substrate) as an additive/promoter [10,11]. The products (gas, liquid and solid) were collected and analyzed as described earlier [10,11].

2.3.2. Regioselective o-hydroxylation

In a typical hydroxylation reaction, the solid catalyst (zeolite-encapsulated copper acetate; CuAc-Y) was added to the substrate in a phosphate buffer (0.05 M, pH 6.5) [22]. The contents were stirred at 298 K in the presence of molecular oxygen for 24 h. The progress of the oxidation was monitored by high-performance liquid chromatography (for L-tyrosine) and gas chromatography (for phenol) [22].

2.3.3. Oxidation of p-xylene

Para-xylene (2 ml), acetic acid (38 ml), distilled water (5.6 ml), NaBr (0.0865 g) and catalyst (Co/Mn cluster encapsulated in zeolite-Y) were taken in a Ti-lined steel Paar reactor which was then pressurized with air at 298 K [15,16]. The reactions were conducted at 473 K and the products were analyzed as described earlier [15,16].

2.3.4. Epoxidation of limonene

Grafted Mn(Salen)Cl (0.1 g), *R*-(+)-limonene (3.75 mmol), *iso*-butyraldehyde (9 mmol), *N*-methyl imidazole (1.7 mmol) and toluene (20 ml) were taken in a double-necked round-bottom flask (50 ml) fitted with a gas-purging unit [18]. The reactions were conducted by bubbling air (1 atm) for 8 h, at 298 K. The catalyst was separated by filtration and the liquid portion was analyzed by gas chromatography [18].

2.3.5. Epoxidation of cyclohexene

Titanosilicate (0.1 g), cyclohexene (0.82 g) and solvent (5 ml) were taken in a glass flask fitted with a water-cooled condenser and placed in a constant temperature oil bath. H_2O_2 ([cyclohexene]/[H_2O_2] = 3 mol/mol) was added drop-wise over a period of 10 min and then the reaction was carried out for 4 h. The products were analyzed by gas chromatography [20]. Some experiments were conducted in the presence of radical scavengers. In those studies a known quantity of the radical scavenger (0.018 mmol) was added to the reaction mixture and the reaction was conducted in a similar manner [20].

3. Results and discussion

3.1. Transition metal complexes encapsulated in zeolite-Y

3.1.1. Selective oxidation of methane and cyclohexane over zeolite-encapsulated metal phthalocyanine complexes

The conversion of methane to methanol is currently achieved by steam reforming or partial oxidation to syngas (CO + H_2) followed by methanol synthesis. The first step of the process is energy intensive while the second step is limited by equilibrium. A single-step, exothermic, direct process to methanol in high yields is desirable. The catalytic oxidation of methane to methanol at high temperatures has been claimed by several authors [23–26]. However, both conversion and methanol selectivity are too low. CO_2 formation is significant at high temperatures. Selective low-temperature oxidation is desirable [27,28]. Metal phthalocyanines (MPc) encapsulated in zeolite-Y exhibit highly efficient catalytic activity at ambient temperatures for the direct oxidation of methane to a mixture of methanol and formaldehyde (Scheme 1) [10]. MPc, with electron withdrawing substituents (like Cl) exhibit higher activity than the unsubstituted MPc complexes (Table 1). The intrinsic catalytic activities of the complexes (TOFs) were enhanced by more than two orders when they were encapsulated (Table 1). Even though methane could be oxidized over these catalysts using O_2 alone, the conversion levels were below 1% and only CO_2 was produced [10]. When both O_2 and *t*-BuOOH were used there was a synergistic enhancement in methane conversion [10]. Similar enhancements in intrinsic catalytic activity/product selectivity of the metal complex on encapsulation were found also in the oxidation of cyclohexane (Scheme 1 and Table 1) [11]. In the Gif system of Barton et al. [29], radical reactions become more important causing over-oxidation and coupling of the products with pyridine. Encapsulated metal phthalocyanines were found to be efficient solid catalysts for the direct oxidation of cyclohexane to adipic acid, in significant yields [30].

"Neat" CoPc possesses a center of inversion (D_{4h} symmetry) (Scheme 1). As a consequence, due to the mutual exclusion principle, the IR-active vibrational modes are absent in the Raman spectra and the Raman modes are absent in the IR spectra of "neat" CoPc complexes [31]. For the zeolite-encapsulated complexes,

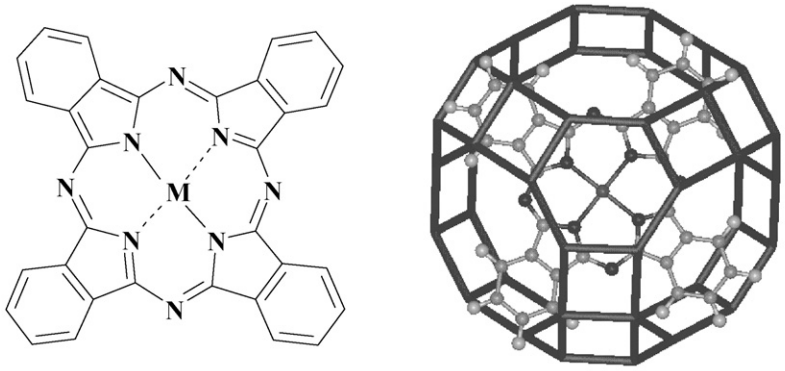

Methane ⟶ **Methanol, formaldehyde, formic acid, carbon dioxide**

Cyclohexane ⟶ **Cyclohexanol, cyclohexanone, adipic acid**

Scheme 1. Molecular structure of "neat" and zeolite-encapsulated metal phthalocyanine and oxidation products of methane and cyclohexane over these catalysts.

however, Ray and Vasudevan [31] found that the Raman-active modes are present even in the IR spectra and *vice versa* implying that the center of inversion in the CoPc molecule had been lost on encapsulation in the zeolite supercages [31]. Magnetic susceptibility measurements revealed that encapsulation lowers the energy difference (Δ; from 351 K for "neat" CoPc to 22 K for CoPc encapsulated in Y) between the higher lying high-spin quartet state (^{4}E) and the low-lying spin-doublet ground state (^{2}B) [31]. Phthalocyanine (Pc) exhibits characteristic π–π^* transitions (Q-bands) in the visible region 550–760 nm [31]. The position and the number of these bands are highly sensitive to the geometry of the molecule. CuPc-Y exhibited four Q-bands that were shifted to lower energy. The red shift and the changes in relative intensities of the Q-bands are probably due to puckering of the planar geometry of Pc due to encapsulation in zeolite-Y [12]. The encapsulated CuPc complexes showed EPR spectra with nine superhyperfine features due to four equivalent nitrogens of the isoindole groups. Hyperfine features due to copper were also resolved (Fig. 1) [12]. Such superhyperfine and hyperfine features were completely absent in the spectra of "neat" CuPc indicating that the intermolecular interactions present in 'neat' CuPc complexes are completely avoided in CuPc-Y as a consequence of "site isolation" on encapsulation [12]. Molecular energy calculations [31] revealed that the introduction of non-planarity decreases the host(zeolite)-guest(phthalocyanine) steric repulsion compensating for the increased internal energy of Pc molecule on distortion. All these structural studies indicate that as a consequence of molecular confinement, the MPc complexes have undergone a change from a planar to a puckered geometry. This change in molecular geometry leads to changes in electronic structure (DRUV–vis and magnetic moment studies) and redox properties of the complex. Such changes in the redox properties, probably, lead to the observed enhanced catalytic activities. Interestingly, metalloenzymes (blue copper proteins, for example) also possess such low-symmetry environments at their active sites [9].

3.1.2. Tyrosinase activity of zeolite-encapsulated copper acetate dimers

Copper acetate (CuAc) encapsulated in zeolite-Y *ortho*-hydroxylates, regioselectively, L-tyrosine to L-dopa and, further, to

Table 1
Selective oxidations over MPc complexes in acetonitrile [10,11]

(A) Oxidation of methane[a]

Catalyst[c]	TOF (min^{-1})[b]	Product selectivity (mol%)		
		CH_3OH	HCHO + HCOOH	CO_2
CoPc	0.08	0	0	100
$CoCl_{16}Pc$	0.41	10.2	87.8	2.0
$CoCl_{16}Pc$-Y (0.27)	30.5	12.5	83.1	4.4
$FeCl_{16}Pc$	0.9	41.2	50.3	8.5
$FeCl_{16}Pc$-X (0.16)	107	52.6	45.5	1.9

(B) Oxidation of cyclohexane[b]

Catalyst[c]	TOF (h^{-1})[b]	Products selectivity (mol%)			
		Cyclohexanol	Cyclohexanone	Adipic acid	Others
CoPc	0.006	41.6	58.4	0	0
$CoCl_{16}Pc$	0.16	13.5	53.6	23.9	22.5
$CoCl_{16}Pc$-X (0.27)	184	19.4	51.1	20.7	8.8
$Cu(NO_2)_4Pc$	0.04	46.1	53.9	0	0
$Cu(NO_2)_4Pc$-X (0.14)	132	78.9	21.2	0	0

[a] Reaction conditions: methane = 50 psi, air = 100 psi, CH_3CN = 99.5 g; catalyst = 0.75 g; *t*-BuOOH = 0.5 g.
[b] Reaction conditions: air—800 psig; reaction time = 8 h; temperature = 353 K.
[c] The catalysts are designated by the following notation: [(complex) – (zeolite) (metal content in the zeolite, wt%)].

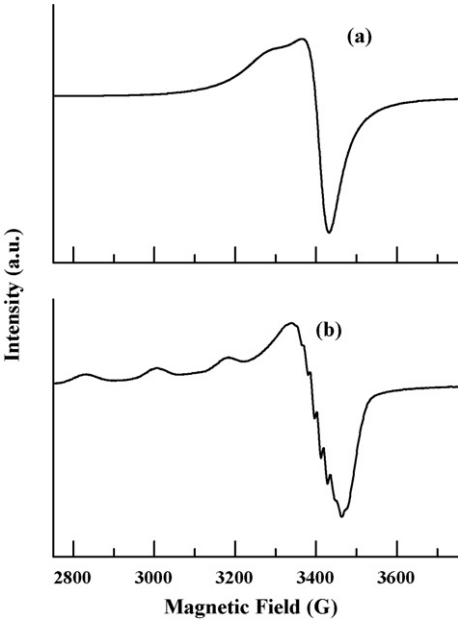

Fig. 1. EPR spectra of "neat" and zeolite encapsulated copper phthalocyanine (CuPc). (a) CuPc and (b) CuPc-Y.

dopaquinone in a phosphate buffer (pH 6.5) at 298 K using atmospheric dioxygen as oxidant (Scheme 2) [22]. The pH specificity as well as the temperature dependence of the reaction suggests that the CuAc complex is active only when it is present as a dimer. When the dimeric structure is absent (lower pH or higher temperatures) the complex is inactive [22]. Oxidation of phenol, for example, yielded only catechol/*o*-benzoquinone; the *para*-isomers, hydroquinone/*p*-benzoquinone were not observed [22]. In all these hydroxylation reactions the encapsulated CuAc dimers exhibited higher catalytic activity than the corresponding "neat" dimer complexes [22].

EPR spectroscopy was used for determining the structure of encapsulated copper acetate molecules. EPR spectra confirmed the presence of CuAc dimers in the supercages of zeolite-Y [13,14]. The spins on the two Cu(II) centers of the dimer ($3d^9$, $S = 1/2$) were coupled anti-ferromagnetically resulting in a ground-state singlet ($S = 0$) and a low-lying excited triplet ($S = 1$) state. At ambient temperatures, the triplet state was also populated and the complex exhibits paramagnetism (1.4 B.M.). As the temperature is lowered (from ambient temperature to 77 K), the excited triplet levels are depopulated and the dimer signal intensity decreased. The exchange interaction between the Cu(II) ions in the dimer increased upon encapsulation from 259 to 310 cm^{-1}; The Cu–Cu distance decreased for the encapsulated CuAc from 2.64 to 2.40 Å [13,14]. The short Cu–Cu distance and the consequent greater, lateral overlap of the Cu orbitals would facilitate the transfer of electron density from the phenolate ligand to the anti-bonding LUMO of the complex thereby, weakening the copper peroxide, O–O bond formed by the coordination of O_2 to the copper complex. Weakening of the O–O bond would, in turn, makes it easier for the cleavage and transfer of one of the two oxygens of the peroxide ligand to a position *ortho* to the phenolate bond [13]. Thus, molecular confinement modifies the structure of the copper acetate dimer and thereby, enhances its catalytic tyrosinase activity.

3.1.3. Aerial oxidation of para-xylene on zeolite-encapsulated Co/Mn clusters

Trinuclear μ_3-oxo, mixed, metal acetato complexes, $[CoMn_2(\mu_3\text{-}O)(CH_3COO)_6(pyridine)_3]$ encapsulated in zeolite-Y (referred to as $CoMn_2(O)$-Y) exhibit high catalytic efficiencies in the selective, aerial oxidation of *para*-xylene to terephthalic acid (Scheme 3) [15,16]. Interestingly, the formation of 4-carboxybenzaldehyde, a worrisome impurity in conventional processes, was suppressed significantly over these solid catalysts. Terephthalic acid is commercially manufactured by using Co and Mn salts, at 473–500 K, in acetic acid solvent using bromide ions as promoters [32]. We had, earlier found that reactive μ_3-oxo Co/Mn mixed clusters are formed in the homogeneous reaction medium [15,16]. These complexes were synthesized and encapsulated inside the supercages of zeolite-Y using the "flexible ligand synthesis" method [15,16]. Studies were performed also on the homonuclear Co and Mn cluster complexes, $Co_3(O)$ and $Mn_3(O)$, respectively. The solid catalyst, $CoMn_2(O)$-Y, at 100% conversion of *para*-xylene, was even more selective (99.4% selectivity for terephthalic acid; with only 0.01% of 4-carboxybenzaldehyde), than the "neat" cluster and conventional homogeneous catalysts (Table 2).

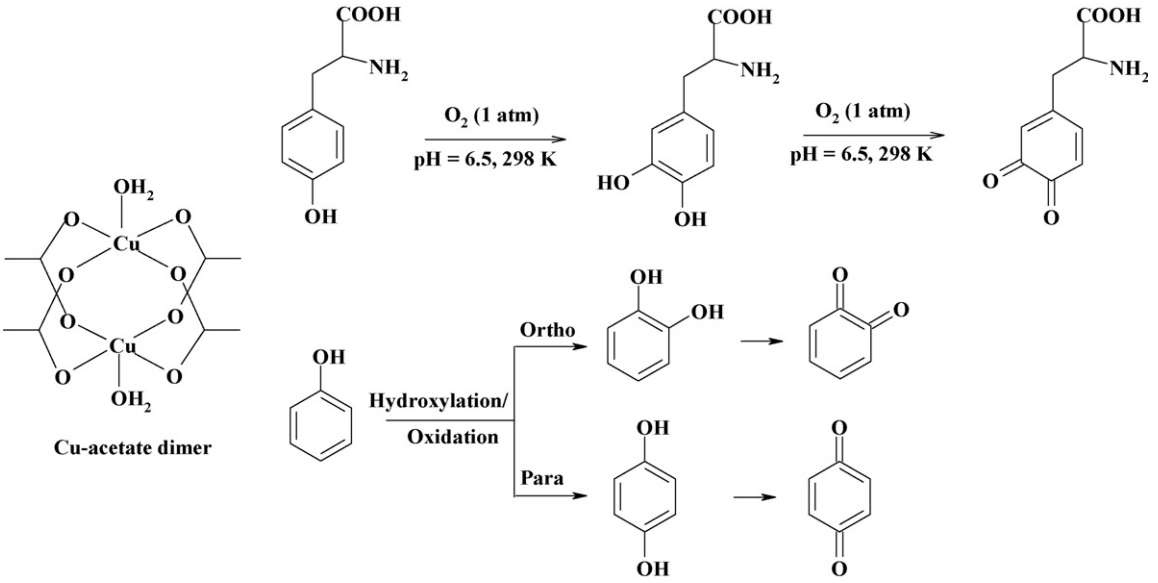

Scheme 2. Structure of copper acetate dimer and *o*-hydroxylation products of tyrosine and phenol.

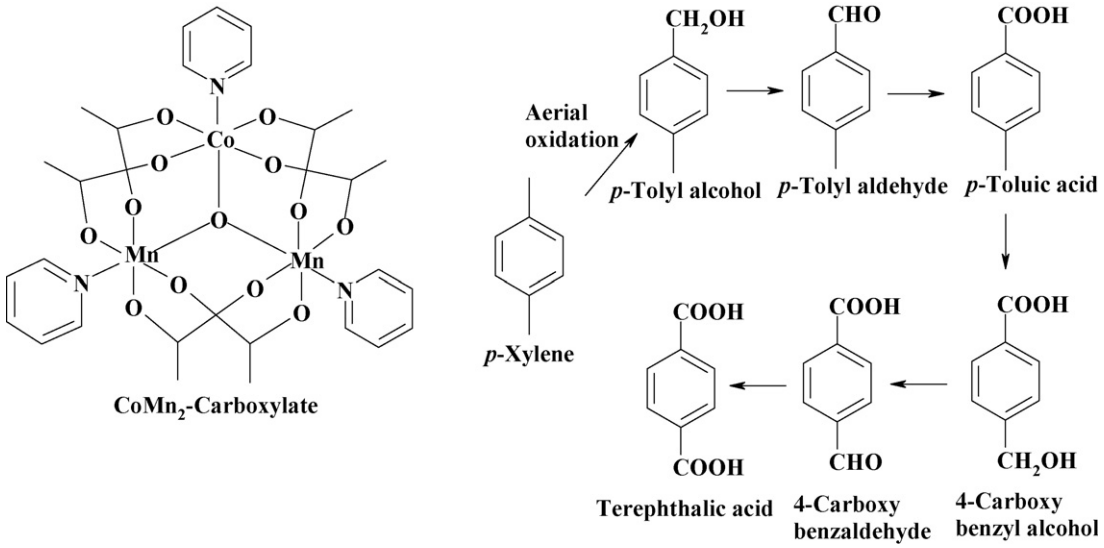

Scheme 3. Oxidation products of *para*-xylene over $[CoMn_2(\mu_3\text{-}O)(CH_3COO)_6(pyridine)_3]$.

Cobalt acetate and $Co_3(O)$ complexes show a redox couple at $E_{1/2}$ values of +0.75 and 0.69 eV, respectively, due to changes in the oxidation state of Co (between +2 and +3) [16]. $CoMn_2(O)$ shows an additional redox couple due to Mn(III)/Mn(IV) in $CoMn_2(O)$. The $E_{1/2}$ value of the redox couple due to Co in $CoMn_2(O)$ occurs at a lower value (+0.56 V) compared to $Co_3(O)$ (+0.69 V) and cobalt acetate (+0.75 V). Lower $E_{1/2}$ values are indicative of a greater ease of electron transfer. The more facile redox behavior of Co in mixed metal Co/Mn cluster catalyst is, possibly, one of the causes for its higher catalytic activity/selectivity. Atomic absorption spectroscopy did not reveal any leaching of metal ions into the liquid portion. However, EPR spectroscopy estimated a leaching of about 0.5% of the encapsulated manganese in the solid catalyst into the solution (about 50 ppm of Mn in solution). This amount cannot account for the observed catalytic activity. Catalytic runs with this trace amount of the metal ions in solution exhibited low *para*-xylene conversions (28 wt%) with *para*-tolyl alcohol and *para*-tolyl aldehyde as products; terephthalic acid was not detected.

3.2. Oxidation of limonene over Mn-Salen grafted on SBA-15

Oxidation of limonene yields a variety of products including carveol and carvone (due to oxidation at allylic C–H bond) and 1,2-epoxide, 8,9-epoxide and 1,2 and 8,9-diepoxides (due to oxidation of the olefinic bond) (Scheme 4). Most of the known solid catalysts (Ti-MCM-41 [33], carbon-anchored $Co(acac)_2$ [34], and supported Keggin heteropoly compounds [35], for example) show significantly low limonene conversions and epoxide selectivities (20–30%); carveol, carvone and polymeric products are formed in large quantities. They require expensive oxidants such as alkyl hydroperoxides and H_2O_2. When using air as an oxidant, sol–gel-prepared Co/SiO_2 [36] yields large amounts of allylic oxidation products. However, the Mukaiyama-type aerial oxidation over Mn(Salen)Cl complexes conducted in the presence of *N*-methyl imidazole (N-MeIm), an additive and *iso*-butyraldehyde, a co-reagent, yielded mainly the epoxide product. The allylic oxidation products were formed only in minor amounts (Table 3) [17,18]. Among the various epoxides, the 1,2-epoxide formed with higher (regio-) selectivity. The immobilized Mn(Salen)Cl complexes exhibited enhanced chemoselectivities than the "neat" complex (Table 3). The selectivity for 1,2-epoxide over different immobilized Mn-complexes in toluene medium increased in the order: SBA-15-*pr*-NH_2-Mn(Salen)Cl (80.2%) < SBA-15-*pr*-SO_3H-Mn(Salen)Cl (82.0%) < SBA-15-*pr*-SH-Mn(Salen)Cl (100%). By hot filtration technique we found that a part of Mn complex leaches out from the solid phase during the oxidation reaction. However, the extent of Mn leaching into the solution decreased in the different catalysts in the order: SBA-15-*pr*-NH_2-Mn(Salen)Cl > SBA-15-*pr*-SO_3H-Mn(Salen)Cl > SBA-15-*pr*-SH-Mn(Salen)Cl.

The Mn ions in "neat" Mn(Salen)Cl are in the trivalent oxidation state and are EPR-silent. Upon immobilization by grafting on functionalized SBA-15, the Mn-complexes became EPR-active and

Table 2
Catalytic activity of Co/Mn cluster complexes in selective oxidation of *para*-xylene [15,16][a]

Catalyst	Reaction time (h)	Xylene conversion (wt%)	Product selectivity (wt%)					
			Para-tolyl alcohol	*Para*-tolyl aldehyde	*Para*-toluic acid	4-Carboxy-benzaldehyde	Terephthalic acid	Benzoic acid
$Co_3(O)$	2	73.1	0.7	32.4	20.4	28.9	16.6	1.0
$Mn_3(O)$	2	77.0	0	35.8	8.6	1.6	53.8	0.2
$CoMn_2(O)$	2	100	0	0	1.8	0.4	97.8	0
$Co_3(O)$-Y	4	69.9	0	28.4	49.5	7.7	12.7	1.7
$Mn_3(O)$-Y	4	99.9	0	0	20.1	0.7	79.2	0
$CoMn_2(O)$-Y	4	100	0	0	0.6	0.01	99.4	0
$Co(CH_3COO)_2 + Mn(CH_3COO)_2$[b]	2	100	0	0	0.7	1.4	97.9	0

[a] Reaction conditions: *para*-xylene (2 ml), NaBr (86.5 mg), H_2O (5.6 ml), acetic acid (38 ml), weight of "neat" cluster catalyst (34.2 mg), weight of encapsulated cluster catalyst (299.5 mg), pressure (550 psig), reaction temperature (473 K), oxidant (air).
[b] Conventional catalyst system: $Co(CH_3COO)_2{\cdot}4H_2O$ (107 mg), $Mn(CH_3COO)_2{\cdot}4H_2O$ (35.7 mg).

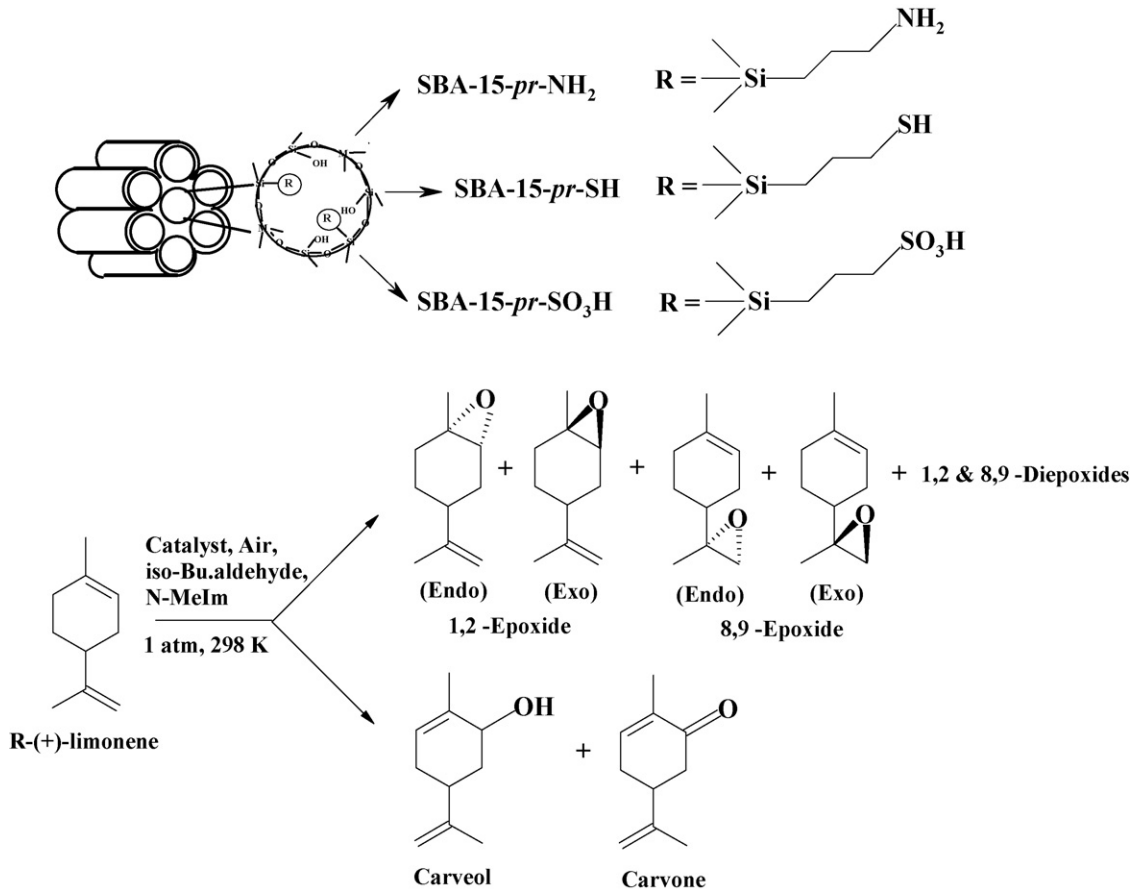

Scheme 4. Grafted Mn(Salen)Cl complexes and oxidation products of limonene.

showed a sextet-line Mn-hyperfine pattern (Fig. 2). The intensity of the Mn signals increased with the acidity of the organo-functional group in the following order: SBA-15-*pr*-NH_2-Mn(Salen)Cl < SBA-15-Mn(Salen)Cl < SBA-15-*pr*-SO_3H-Mn(Salen)Cl < SBA-15-*pr*-SH-Mn(Salen)Cl. While the *g*-values of these systems are similar (g_{av} = 2.0010), the hyperfine coupling constant (A), representing the electron density at the site of manganese, was modified considerably. The A value for SBA-15-*pr*-NH_2-Mn(Salen)Cl was 88.4 G while that for SBA-15-*pr*-SH-Mn(Salen)Cl was 96 G. The appearance of these EPR signals, characteristic of Mn^{2+}, indicates that, at least, a portion of the Mn ions is reduced from +3 to +2 oxidation state upon immobilization on the functionalized SBA-15 surface. In SBA-15-*pr*-SH-Mn(Salen)Cl, wherein the electron density at Mn is higher (A_{Mn} = 96 G), such a reduction from +3 to +2 oxidation state is more favored and, as a consequence, more intense EPR signals were detected (Fig. 2).

The solid immobilized catalysts showed a distinct redox couple in the cyclic voltammogram attributable to Mn^{+4}/Mn^{3+} transitions [18]. The $E_{1/2}$ value of this couple for different Mn-catalysts increased in the following order: SBA-15-*pr*-SH-Mn(Salen) (+0.643 V) < SBA-15-*pr*-SO_3H-Mn(Salen)Cl (+0.682 V) < SBA-15-*pr*-NH_2-Mn(Salen)Cl (+0.705 V) [18]. Lower $E_{1/2}$ values are indicative of more facile oxidation and reduction. Hence, a Mn-complex immobilized on a propylthiol-functionalized support is more easily oxidized/reduced than when supported on propylsulfonic acid or propylamine-functionalized SBA-15 support. These results agree well with the observations from EPR spectroscopy. The acidity of the support, therefore, influences the electronic structure and redox behavior of the immobilized complex. Interestingly, the variation in epoxide selectivity follows the variation in electron density (hyperfine coupling constant—A; see EPR data) and oxidizability (see cyclic voltammetric data) of the

Table 3
Aerial oxidation of *R*-(+)-limonene over "neat" and immobilized Mn(Salen)Cl complexes [18]

Catalyst	*R*-(+)-limonene conversion (mol%)	TOF (h^{-1})[a]	Product selectivity (mol%)				
			1,2-Epoxide	8,9-Epoxide	1,2 and 8,9-diepoxide	Carveol	Carvone
"Neat" Mn(Salen)Cl	69.2	7.0	74.2	7.2	6.2	5.2	7.2
SBA-15-*pr*-NH_2-Mn(Salen)Cl	75.9	35.4	80.2	6.4	7.2	4.0	2.2
SBA-15-*pr*-SO_3H-Mn(Salen)Cl	60.0	17.8	82.0	8.0	2.6	3.7	3.7
SBA-15-*pr*-SH-Mn(Salen)Cl	64.1	58.9	100	0.0	0.0	0.0	0.0

Reaction conditions: *R*-(+)-limonene = 3.75 mmol; catalyst = 0.0165 g ("neat") or 100 mg ("immobilized"); *iso*-butyraldehyde = 9 mmol; N-MeIm = 1.7 mmol; oxidant—air = 1 atm (2 ml/min); toluene = 20 ml; reaction temperature = 298 K; reaction time = 8 h.
[a] Turnover frequency (TOF) = moles of *R*-(+)-limonene converted per mole of Mn per hour. The Mn contents in SBA-15-*pr*-NH_2-Mn(Salen)Cl, SBA-15-*pr*-SO_3H-Mn(Salen)Cl and SBA-15-*pr*-SH-Mn(Salen)Cl are 0.6, 0.9 and 0.3 wt%, respectively.

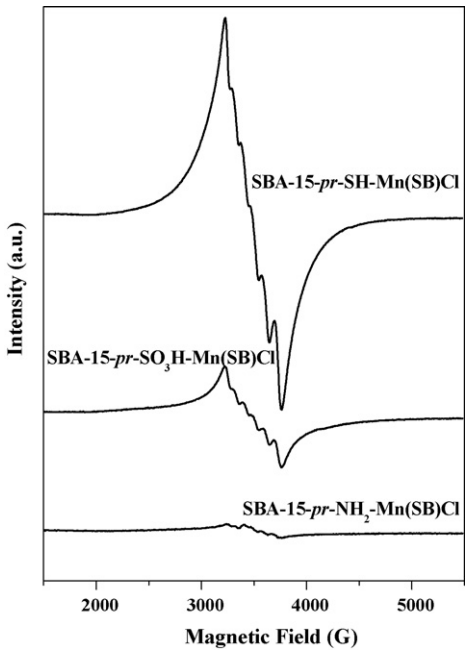

Fig. 2. EPR spectra (77 K) of Mn(SB)Cl immobilized on different SBA-15 supports. SB = Salen.

Mn ions. The Mn-complexes immobilized on propylthiol-functionalized SBA-15 exhibited higher catalytic activity (turnover frequency; TOF) than those immobilized on propylsulfonic acid and propylamine-functionalized SBA-15 supports (Table 3). Apparently, supports on which Mn ions are more easily oxidizable are lead to more selective oxidation catalysts.

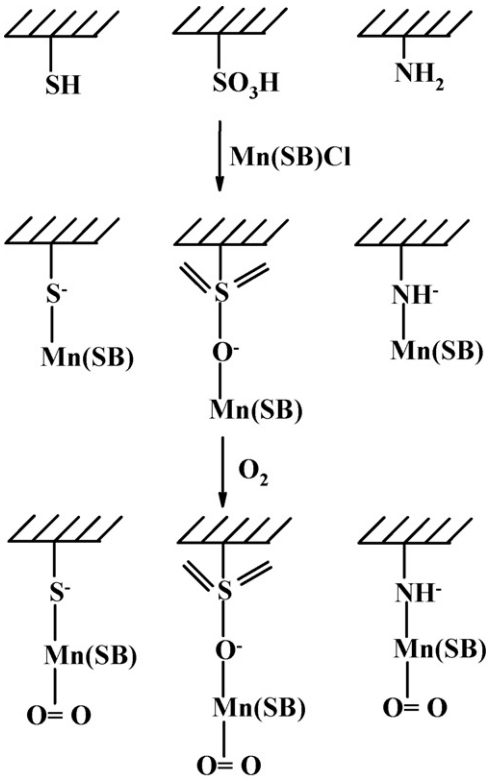

Scheme 5. Reactive oxo-Mn species in grafted Mn(Salen)Cl complexes.

Based on the magnitude of Mn hyperfine coupling constants, which is an indication of the electron density at the site of Mn, the metal–ligand (sulfur/oxygen/nitrogen) bond strength in different grafted Mn(Salen) complexes would decrease in the order: SBA-15-*pr*-SH-Mn(Salen)Cl > SBA-15-*pr*-SO_3H-Mn(Salen)Cl > SBA-15-*pr*-NH_2-Mn(Salen)Cl (Scheme 5). Due to *trans*-axial lability, the Mn–O_2 bond strength (in the oxygen adduct) should increase in the reverse order. Thereby, the O–O bond strength of the activated oxygen should follow the same order while the electron density on oxygen orbitals follows the reverse trend: SBA-15-*pr*-SH-Mn(Salen)Cl < SBA-15-*pr*-SO_3H-Mn(Salen)Cl < SBA-15-*pr*-NH_2-Mn(Salen)Cl. Heterolytic O–O bond cleavage, formation of reactive Mn=O and the consequent epoxide selectivity are therefore expected to be higher in SBA-15-*pr*-SH-Mn(Salen)Cl than in SBA-15-*pr*-SO_3H-Mn(Salen)Cl and SBA-15-*pr*-NH_2-Mn(Salen)Cl. Thus, higher electron density at manganese (due to reduction from +3 to +2 state) and consequent lower redox potential of grafted Mn complex enhance catalytic activity. The ability to fine tune redox potential of grafted metal complexes (and thereby, their catalytic oxidation properties) by modifying surface charge/potential is a powerful tool in the design of solid oxidation catalysts. In Table 3, the first and the last entries for the "neat" and SBA-15-*pr*-SH-grafted Mn(Salen)Cl, have similar limonene conversions but the turnover frequency (TOF) values are different by almost an order of magnitude. Further the selectivity for 1,2-epoxide over SBA-15-*pr*-SH-Mn(Salen)Cl is remarkably high (100%). This is primarily because of the difference in the oxidation states of Mn in the "neat"

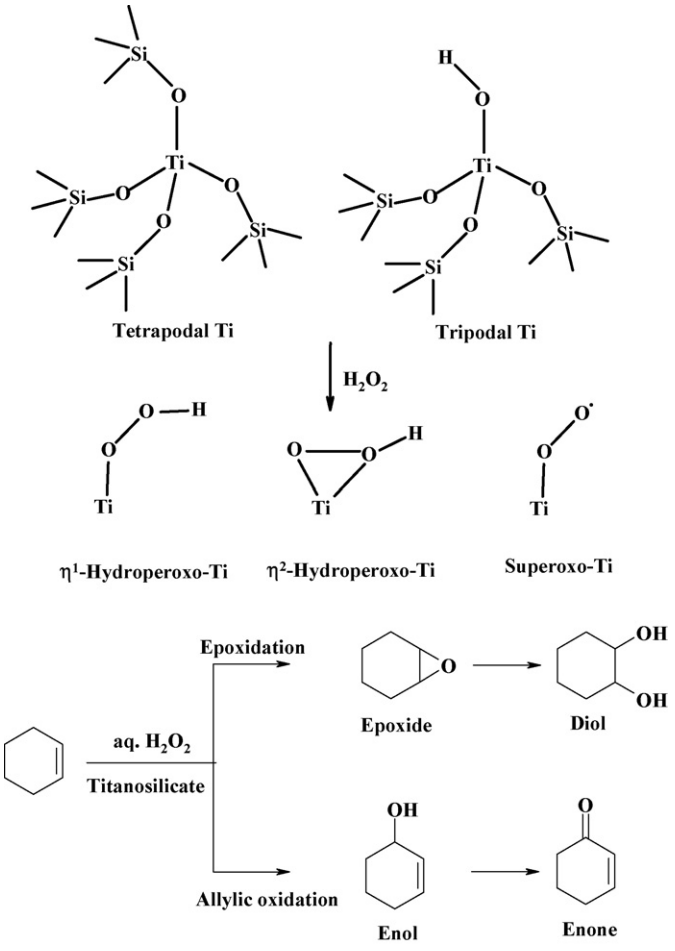

Scheme 6. Ti structures and reactive oxo-Ti species in titanosilicates. Oxidation products of cyclohexene.

and grafted complexes. As mentioned before, Mn is in a +3 oxidation state in the "neat" complex. Upon grafting on surface thiol groups, the electronic structure is modified and the oxidation state of Mn is reduced from +3 to +2. This is an example where the support has shown a definite influence on the electronic structure, and, thereby on the catalytic activity/selectivity of the grafted Mn complexes.

3.3. Selective oxidations over transition metal ions in framework positions

Several metal ions including Fe^{3+}, Ti^{4+}, $V^{4+/5+}$, Sn^{4+} and $As^{3+,5+}$ have been incorporated in zeolites and silica matrices. Among them, the titanosilicates (with Lewis acidic Ti sites) show remarkable catalytic activity for the oxidation of alkanes, olefins, aromatics, ammonia/amines and sulfur-containing compounds with molecular oxygen, hydrogen peroxide or t-BuOOH at mild conditions [37]. XANES and EXAFS studies have revealed that there exist two major types of tetracoordinated Ti structures—tetrapodal Ti coordinated to four SiO^- groups and a tripodal Ti coordinated to three SiO^- and one HO^- group (Scheme 6). Concentrations of those Ti species depend on the zeolite structure. While the tetrapodal Ti shows a characteristic UV-band at around 210 nm, the tripodal Ti shows the band at 220 nm [37]. They can be discriminated also by their redox potentials. Tripodal Ti ions are more easily reducible than tetrapodal Ti. EPR studies of titanosilicates reacted with hydrogen at elevated temperatures further confirmed this conclusion [37]. It is also likely that certain amorphous materials like, Ti-MCM-41, also contain the bipodal Ti coordinated to two SiO^- and two OH^- groups. However, these defect Ti species are unstable and usually leach out during the oxidation reaction. Well-prepared samples, thus, contain mainly the tetra and tripodal Ti species only.

Reactive oxo-Ti species (peroxo-, hydroperoxo- and superoxo-Ti) on titanosilicates (Scheme 6) were generated by contacting H_2O_2, ($H_2 + O_2$) or *t*-BuOOH. XANES studies provided evidence for the formation of hydroperoxo/peroxo-Ti species [37]. EPR spectroscopy gave evidence for the presence of superoxo-Ti species [19–21]. The hydroperoxo/peroxo and superoxo-Ti could be discriminated based on their DRUV–vis spectral pattern [37]. Both EPR and DRUV–vis spectral techniques confirm that all these oxo-species are in equilibrium during the oxidation reaction and their concentration depends on the temperature, pH, solvent and structural features like the geometry and redox potential of the Ti^{4+} ions. Detailed EPR studies revealed that at least two types (A and B) of superoxo-Ti species are generated on different titanosilicates (Fig. 3). The A-type superoxo-Ti originates from the tetrapodal Ti sites and the B-type from the tripodal-Ti sites. Both A and B-type superoxo-Ti species were detected on TS-1; the former being more abundant than the latter. Ti-MCM-41 contained mainly the latter, type B, superoxo-Ti species (Fig. 3). Based on the EPR g-parameters of superoxo-Ti species we had estimated the energy gap (Δ) between the π_x^* and π_y^* orbitals which is sensitive to the coordination and covalency of the Ti–O_2 bond [19–21]. The g_z value of different Ti($O_2^{\bullet -}$) species decrease in the order: A-type > B-type. The Δ values vary in the reverse order. Hence, the strength of the Ti-O bond increases in the order: A-type < B-type. The O–O bond strength follows the reverse order. Hence, the A-type species having lower amount of electron density on oxygen orbitals lead to heterolytic O–O bond cleavage resulting in ionic oxo-intermediates while the B-type oxo-Ti species leads to homolytic O–O bond cleavage resulting in radical oxo-intermediates. The type A species is, probably, the active intermediate in epoxidations while B leads to non-selective oxidations. TS-1 generates type A species in greater abundance than Ti-MCM-41 and Ti-SBA-15; the latter generate mostly the type B species from H_2O_2. The greater epoxidation selectivity of TS-1 (compared to Ti-MCM-41 and Ti-SBA-15) probably arises from this crucial difference.

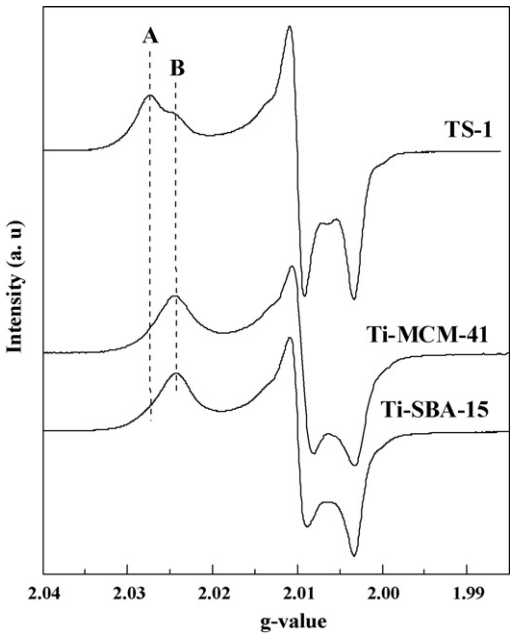

Fig. 3. Typical EPR spectra (at 80 K) of superoxo-Ti in different titanosilicates contacted with aq. H_2O_2. The g_{zz} signals corresponding to different superoxo species (A and B) are indicated.

To confirm this point, we have used radical traps (like hydroquinone) during epoxidation of cyclohexane with H_2O_2 over TS-1 and Ti-SBA-15 catalysts [20]. When the reaction was conducted without a radical trap, epoxide, diol, cyclohexanol and cyclohexanone were all formed as products (Scheme 6 and Table 4). The selectivity for (diol + -ol + -one) is higher on Ti-SBA-15 than on TS-1. Mesoporous titanosilicates containing predominantly the tripodal Ti and generating type B oxo-Ti species produced more amounts of allylic oxidation products. When the reaction was conducted in the presence of a small amount of hydroquinone (radical trap), the selectivity for epoxide increased significantly [20]. All the radical oxo-intermediates formed via homolysis of the O–O bond (giving rise to allylic oxidation

Table 4
Epoxidation of cyclohexene over TS-1 and Ti-SBA-15: influence of hydroquinone (HQ) [20][a]

Catalyst	HQ	Cyclohexene conv. mol% (theoretical)[b]	Product selectivity (mol%)		
			Epoxide	Diol	Allylic oxidation (-ol + -one)
TS-1	No	18.6	55.5	28.8	15.7
	Yes	15.3	100	0.0	0.0

[a] Reaction conditions: catalyst, 100 mg; cyclohexene, 10 mmol; HQ, 0 or 0.018 mmol; H_2O_2 (30% aqueous), 3.33 mmol; CH_3CN, 5 ml; temperature, 333 K; reaction time, 4 h.
[b] Cyclohexene conversion (mol%): theoretical = experimental conversion (mol%) × moles of cyclohexene taken/moles of H_2O_2 added.

products) are trapped by the radical trap-hydroquinone increasing the selectivity for the epoxide. Interestingly the diol formation is completely suppressed (Table 4). While the possible reason for this is not clear, it may be noted that the addition of a small quantity of a radical trap like hydroquinone significantly improves the chemoselectivity in oxidation reactions.

4. Conclusions

Selective oxidations of hydrocarbons in the liquid phase are reported over three categories of zeolite and mesoporous silica-based catalysts: (1) transition metal complexes (metal phthalocyanine, copper acetate dimer and Co/Mn acetate trimer) encapsulated in zeolite-Y, (2) transition metal complexes like Mn-salen, grafted on mesoporous silica molecular sieves, like SBA-15, and (3) transition metal ions, like Ti in framework positions of zeolites and mesoporous molecular sieves. The studies on encapsulated metal complexes reveal that geometric distortions and consequent changes in energy levels and redox potential modify the catalytic oxidation activity. The surface ligands (-*pr*-NH_2, -*pr*-SH and –*pr*-SO_3H) modify the redox potential and oxidation activity/selectivity of Mn(salen) complexes. Electron density at framework Ti and Ti-oxo species influence the mode of O–O cleavage (heterolytic/homolytic) and product selectivity. Our studies suggest that by an appropriate choice of the metal species, support structure, surface acidity and metal–support interactions, one should be able to design, at least, in principle, highly active and selective heterogeneous oxidation catalysts.

Acknowledgments

Authors thank the contributions of Drs. R. Raja, S.A. Chavan, V.N. Shetti and Mr. L. Saikia to this work.

References

[1] K.J. Balkus Jr., A.G. Gabrielov, J. Incl. Phenom. Mol. Recog. Chem. 21 (1995) 159.
[2] D.E. De Vos, M. Dams, B.F. Sels, P.A. Jacobs, Chem. Rev. 102 (2002) 3615.
[3] D. Brunel, N. Bellocq, P. Sutra, A. Cauvel, M. Lasperas, P. Moreau, F. Di Renzo, A. Galarneau, F. Fajula, Coord. Chem. Rev. 178–180 (1998) 1085.
[4] R.F. Parton, I. Vankelecom, C.P. Bezoukhanova, M. Casselman, J. Uytterhoeven, P.A. Jacobs, Nature 370 (1994) 541.
[5] P.P. Knops-Gerrits, D.E. De Vos, F. Thibault-Starzyk, P.A. Jacobs, Nature 369 (1994) 543.
[6] Y.V.S. Rao, D.E. De Vos, T. Bein, P.A. Jacobs, Chem. Commun. (1997) 355.
[7] M.J. Sabater, A. Corma, A. Domenech, V. Fornes, H. Garcia, Chem. Commun. (1997) 1285.
[8] P. Piaggio, P. McMorn, C. Langham, D. Bethell, P.C. Bulman-Page, F.E. Hancock, G.J. Hutchings, New J. Chem. (1998) 1167.
[9] Metal sites in proteins and models: Iron centers, H.A.O. Hill, P.J. Sadler, A.J. Thomson (Eds.), Structure & Bonding, vol. 88, Springer-Verlag, Berlin, 1997.
[10] R. Raja, P. Ratnasamy, Appl. Catal. A: Gen. 158 (1997) L7.
[11] R. Raja, P. Ratnasamy, Catal. Lett. 48 (1997) 1.
[12] S. Seelan, A.K. Sinha, D. Srinivas, S. Sivasanker, J. Mol. Catal. A: Chem. 157 (2000) 163.
[13] S.A. Chavan, D. Srinivas, P. Ratnasamy, Topics Catal. 11 (12) (2000) 359.
[14] S.A. Chavan, D. Srinivas, P. Ratnasamy, J. Catal. 192 (2000) 286.
[15] S.A. Chavan, D. Srinivas, P. Ratnasamy, Chem. Commun. (2001) 1124.
[16] S.A. Chavan, D. Srinivas, P. Ratnasamy, J. Catal. 204 (2001) 409.
[17] L. Saikia, D. Srinivas, P. Ratnasamy, Appl. Catal. A: Gen. 309 (2006) 144.
[18] L. Saikia, D. Srinivas, P. Ratnasamy, Microporous Mesoporous Mater. 104 (2007) 225.
[19] D. Srinivas, P. Manikandan, S.C. Laha, R. Kumar, P. Ratnasamy, J. Catal. 217 (2003) 160.
[20] V.N. Shetti, D. Srinivas, P. Ratnasamy, Zeits. Für Physik. Chem. 219 (2005) 905.
[21] V.N. Shetti, P. Manikandan, D. Srinivas, P. Ratnasamy, J. Catal. 216 (2003) 461.
[22] R. Raja, P. Ratnasamy, J. Mol. Catal. A: Chem. 100 (1995) 93.
[23] US Patent No. 5,220,080.
[25] US Patent No. 5,347,057.
[26] US Patent No. 5,406,017.
[27] L.C. Kao, A.C. Hutson, A. Sen, J. Am. Chem. Soc. 113 (1991) 700.
[28] R.A. Periana, D.J. Tanbe, E.R. Evitt, D.G. Loffler, P.R. Wertreck, G. Voss, T. Masuda, Science 259 (1993) 340.
[29] D.H.R. Barton, F. Halley, N. Ozbalik, M. Schmilt, E. Yound, G. Balavoine, J. Am. Chem. Soc. 111 (1989) 7144.
[30] R.F. Parton, I.F.J. Vankelcom, M.J.A. Casselman, C.P. Bezouhanova, J.B. Utterhoeven, P.A. Jacobs, Nature 570 (1994) 541.
[31] S. Ray, S. Vasudevan, Inorg. Chem. 42 (2003) 1711.
[32] W. Partenheimer, Catal. Today 23 (1995) 65.
[33] R. Hutter, T. Mallat, A. Baiker, J. Catal. 153 (1995) 177.
[34] P. Oliveira, A.M. Ramos, I. Fonseca, A. Botelho do Rego, J. Vital, Catal. Today 102–103 (2005) 67.
[35] H.E.B. Lempers, R.A. Sheldon, Appl. Catal. A: Gen. 143 (1996) 137.
[36] P.A. Robles-Dutenhefner, M.J. da Silva, L.S. Sales, E.M.B. Sousa, E.V. Gusevskaya, J. Mol. Catal. A: Chem. 217 (2004) 139.
[37] P. Ratnasamy, D. Srinivas, H. Knözinger, Adv. Catal. 48 (2004) 1.